Engineering Geology 179 (2014) 102–116

Contents lists available at ScienceDirect

Engineering Geology

journal homepage: www.elsevier.com/locate/enggeo

Simplified quantitative risk assessment of rainfall-induced landslides modelled by infinite slopes

Abid Ali [a,*], Jinsong Huang [a], A.V. Lyamin [a], S.W. Sloan [a], D.V. Griffiths [a,b], M.J. Cassidy [a,c], J.H. Li [c]

[a] ARC Centre of Excellence for Geotechnical Science and Engineering, The University of Newcastle, Callaghan, NSW 2308, Australia
[b] Department of Civil and Environmental Engineering, Colorado School of Mines, Golden, CO 80401, USA
[c] ARC Centre of Excellence for Geotechnical Science and Engineering, The University of Western Australia, Crawley, WA 6009, Australia

ARTICLE INFO

Article history:
Received 12 February 2014
Received in revised form 20 June 2014
Accepted 30 June 2014
Available online 8 July 2014

Keywords:
Consequence
Triggering mechanism
Landslide
Rainfall
Risk
Random field

ABSTRACT

Rainfall induced landslides vary in depth and the deeper the landslide, the greater the damage it causes. This paper investigates, quantitatively, the risk of rainfall induced landslides by assessing the consequence of each failure. The influence of the spatial variability of the saturated hydraulic conductivity and the nature of triggering mechanisms on the risk of rainfall-induced landslides (for an infinite slope) are studied. It is shown that a critical spatial correlation length exists at which the risk is a maximum and the risk is higher when the failure occurs due to a generation of positive pore water pressure.

1. Introduction

Landslides cause damage to buildings, infrastructure, agricultural land and crops. In the majority of cases the main trigger for landslides is heavy or prolonged rainfall (Brand, 1984; Fourie, 1996). Rainfall-induced landslides are common in tropical and subtropical regions where residual soils exist in slopes and there are negative pore water pressures in the unsaturated zone above the water table (Rahardjo et al., 1995). In an unsaturated soil, these negative pore water pressures contribute towards its shear strength and thus help to maintain stability (Fredlund and Rahardjo, 1993). The infiltration of rainwater causes a reduction in this negative pore water pressure and an increase in the soil unit weight (due to an increased saturation), both of which have a destabilizing influence.

Research on rainfall-induced slope failure indicates that several factors affect the stability of a slope subjected to rainfall infiltration. Published research in the area (Zhang et al., 2011; Zhan et al., 2012; Li et al., 2013) shows that the rainfall characteristics (duration, intensity and pattern), the saturated hydraulic conductivity of the soil, the slope geometry, the initial conditions, and the boundary conditions are the factors that influence the stability of a slope subjected to rainfall. Among these factors, the hydraulic conductivity is a very important parameter in seepage and stability problems involving unsaturated soils (Tsaparas et al., 2002; Rahardjo et al., 2007; Rahimi et al., 2010).

Most studies involving rainfall-induced landslides are deterministic in nature, where the soil is assumed to be homogeneous and averaged (or design) soil properties are considered in the analysis (Gui et al., 2000). The uncertainties associated with the soil parameters are usually dealt with by adopting "reasonably averaged" parameters, coupled with practical experience (Duncan, 1996). In reality, soil is inherently heterogeneous with its properties varying from point to point due to different depositional and post-depositional processes (DeGroot and Baecher, 1993; Lacasse and Nadim, 1996). A few studies focused on the effects of the spatial variability of the hydraulic conductivity on rainfall infiltration and subsequent slope stability by using random field theory (e.g. Santoso et al., 2011; Zhu et al., 2013; Cho, 2014), but those studies did not investigate the nature of the triggering mechanism or quantified the risk associated with a rainfall-induced landslide when the saturated hydraulic conductivity varies spatially.

It is now commonly believed that there are two mechanisms that trigger failure in slopes subject to rainfall infiltration (Li et al., 2013); loss of suction during propagation of the wetting front and the rise of the water table (which generates a positive pore water pressure).

Generally, a loss of suction (i.e. reduction in negative pore water pressure) causes a shallow failure while a rise in the water table (i.e. generation of a positive pore water pressure) causes a deep failure. However, this may not be true when the saturated hydraulic conductivity varies spatially, as the water may accumulate at shallow depths

* Corresponding author. Tel.: +61 2 4985 4974.
E-mail address: abid.ali@uon.edu.au (A. Ali).

http://dx.doi.org/10.1016/j.enggeo.2014.06.024
0013-7952/

(Huang et al., 2010) leading to a positive pore water pressure and a shallow failure. To the authors' knowledge, this important effect has not been studied systematically. Another key aspect of the risk assessment of rainfall-induced landslides is the assessment of consequence. Rainfall-induced landslides can be shallow or deep. It is clear that a deep-seated landslide will tend to cause more damage and thus has a more severe consequence. Therefore, the consequence associated with a shallow or deep failure should be assessed individually.

The changes in the near-surface pore water pressures caused by rainfall may be determined using field-observations, analytical solutions or numerical methods. This steady-state pore-pressure field is then used to determine the slope stability either analytically or numerically. Among these uncoupled approaches, the infinite slope model combined with a one-dimensional hydrological model is popular (e.g. Collins and Znidarcic, 2004; Tsai and Chen, 2010; Tsai, 2011; White and Singham, 2012; Zhan et al., 2012; Zhang et al., 2012; Li et al., 2013; Zhang et al., 2014) and will be adopted in this study. In the infinite slope model, the landslide is characterized as a slope failure occurring along a plane parallel to the ground surface. It assumes that each slice of an infinitely long slope receives the same amount and intensity of rainfall (Collins and Znidarcic, 2004); that the time required for infiltration normal to the slope is much less than the infiltration time required for flow parallel to the slope; that the wetting front propagates in a direction normal to the slope[1] (White and Singham, 2012); and that the depth of failure is small compared to the length of the failing soil mass. The validity of these assumptions has been checked against the predictions of two-dimensional numerical models, with the conclusion that an infinite slope approximation may be adopted as a simplified framework to assess failures due to the infiltration of rainfall (Zhan et al., 2012; Li et al., 2013).

In this study, the saturated hydraulic conductivity is modelled as a random field and coupled with Monte-Carlo simulations for the determination of failure probability, consequence and risk. The rainfall-induced landslide risks of two slopes having different triggering mechanism are studied by adopting the quantitative risk assessment framework proposed by Huang et al. (2013). To obtain the pore water distributions, the modified form of one-dimensional Richards equation (Richards, 1931) is solved numerically by the HYDRUS 1D software (Simunek et al., 2013).

2. Seepage analysis

Assuming that the effect of pore-air pressure is insignificant and that water flow due to thermal gradients is negligible, one-dimensional uniform flow in a variably saturated soil can be described by a modified form of Richards equation (Richards, 1931). Therefore, the flow in an unsaturated infinite soil slope can be described by the 1D equation (e.g. Zhan et al., 2012):

$$\frac{d\theta}{dt} = \frac{d}{dz}\left(K\left[\frac{du}{dz} + \cos\alpha\right]\right) \tag{1}$$

where θ is the volumetric water content, t is time, u is the pore water pressure head, α is the inclination of the slope to the horizontal, K is the hydraulic conductivity and z is the spatial coordinate as shown in Fig. 1. To solve the above equation numerically, the water content θ is assumed to vary with the pore water pressure head u according to the van Genuchten (1980) model as:

$$S_e = \frac{\theta-\theta_r}{\theta_s-\theta_r} = \left[\frac{1}{1+(au)^N}\right]^m \tag{2}$$

where S_e is the effective degree of saturation, θ_s and θ_r are the saturated and residual water content respectively, a is the suction scaling parameter and N, m are the parameters of the van Genuchten model. Noting that the volumetric water content is related to the degree of saturation S and the porosity n (by the relation $\theta = nS$), the effective degree of saturation can also be expressed in terms of the degree of saturation S in the following form:

$$S_e = \frac{S-S_r}{1-S_r} \tag{3}$$

where S_r is the residual degree of saturation. To complete the description, the hydraulic conductivity K can be estimated as:

$$K = K_s K_r \tag{4}$$

where K_s is the saturated hydraulic conductivity and K_r is the relative hydraulic conductivity given by van Genuchten (1980):

$$K_r = S_e^{1/2}\left[1-\left(1-S_e^{1/m}\right)^m\right]^2. \tag{5}$$

In this study, the saturated hydraulic conductivity is modelled as a random field and Eq. (1) is solved by HYDRUS 1D. The distribution of pore water pressure and the degree of saturation are then used in the infinite slope model to assess the slope stability.

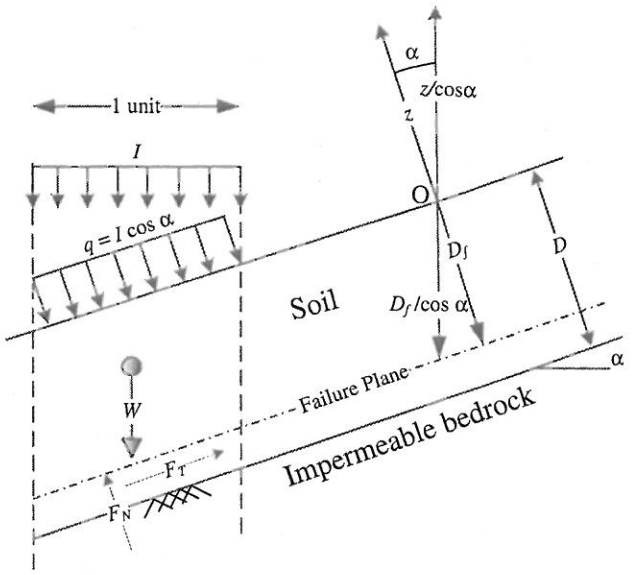

Fig. 1. Limit-equilibrium set up.

2.1. Slope stability assessment

Once the pore water pressure distribution is obtained through seepage analysis, the factor of safety FS at any given time t can then be determined by limit-equilibrium techniques. The stability of an infinite slope is estimated by using a closed form solution similar to that proposed by White and Singham (2012), where the failure is considered to occur along a plane parallel to the ground surface. A soil column of a unit width is considered, where the self-weight W is used to obtain the normal force F_N and tangential force F_T at any depth. The expression

[1] The use of an infinite slope model implies that the pore water pressure at a certain depth is same along all lateral extents of the slope i.e. the pore pressure contours are parallel to the ground surface when the slope is subjected to rainfall (e.g. Zhan et al., 2012). Pore pressure contours parallel to the ground surface also imply that any variability in the hydraulic conductivity (parallel to the slope surface) is neglected. If flow is not strictly one-dimensional, then the pore water pressures will vary along the lateral extent of the slope, even at the same depth. The problem in such a case will no longer be one-dimensional in nature and the use of an infinite slope model would be inappropriate.

for the factor of safety is derived along the same lines as White and Singham (2012).

Referring to Fig. 1, resolving equilibrium of the normal forces on the slip plane gives:

$$F_N = W\cos\alpha \tag{6}$$

where W is the self-weight of the soil column above the failure plane. The unit weight of soil during rainfall infiltration will increase due to an increase in water content; neglecting this effect (i.e. assuming a constant unit weight) could lead to a higher (and thus false) estimate of stability (Tsai and Chen, 2010; Zhan et al., 2012). Therefore, to account for the variation in unit weight due to the variation in the water content with depth, W is determined as:

$$\begin{aligned} W &= \int_0^{D_f/\cos\alpha} \gamma \frac{dz}{\cos\alpha} = \frac{1}{\cos\alpha}\int_0^{D_f/\cos\alpha} [(1-n)\gamma_s + nS\gamma_w]dz \\ &= \frac{1}{\cos\alpha}\int_0^{D_f/\cos\alpha} [(1-n)\gamma_s + \theta\gamma_w]dz \end{aligned} \tag{7}$$

where D_f is the failure depth, γ is the bulk unit weight of soil, γ_s is the unit weight of soil solids, and γ_w is the unit weight of water and the water content θ is defined in Eq. (2). Note that the integration takes place along the vertical direction as illustrated in Fig. 1. From simple statics, the total normal stress σ on the failure surface can be computed as:

$$\sigma = F_N\cos\alpha \tag{8}$$

$$\sigma = W\cos^2\alpha \tag{9}$$

while the corresponding shear force is given by:

$$F_T = W\sin\alpha. \tag{10}$$

Hence the shear stress on the failure surface is:

$$\tau = F_T\cos\alpha \tag{11}$$

or

$$\tau = W\cos\alpha\sin\alpha. \tag{12}$$

In this study, the shear strength of soil τ_f (in terms of effective stress) is assumed to be described by the Mohr–Coulomb model:

$$\tau_f = c' + \sigma'\tan\left(\phi'\right) \tag{13}$$

where c' is the effective cohesion, σ' is the effective normal stress, and ϕ' is the effective friction angle. To consider the influence of pore water pressure on the shear strength of a variably saturated soil, Terzaghi's effective stress principle is modified according to the formulation of Bishop (1959):

$$\sigma' = (\sigma - u_a) + \chi(u_a - u_w) \tag{14}$$

where u_a is the pore-air pressure, $u_w = \gamma_w u$ is the pore water pressure, $(u_a - u_w)$ is known as matric suction and χ is called the coefficient of effective stress and is a constitutive property of the soil that depends on the degree of saturation. For a variably saturated soil, χ denotes the proportion of matric suction that contributes to the effective stress and generally varies between 0 (for a perfectly dry soil) and 1 (for a completely saturated soil). Though many mathematical forms of χ have been proposed in the past, in the present study χ is considered equal to the effective degree of saturation, S_e (Vanapalli et al., 1996):

$$\chi = \frac{\theta-\theta_r}{\theta_s-\theta_r} = \frac{S-S_r}{1-S_r} = S_e. \tag{15}$$

Substituting $u_a = 0$ in Eq. (14) and substituting Eq. (15) in Eq. (14) gives:

$$\sigma' = \sigma - S_e u_w. \tag{16}$$

Slope failure occurs when the applied shear stress τ exceeds the mobilized soil shear strength τ_f. The factor of safety FS can then be computed as:

$$FS = \frac{\tau_f}{\tau} = \frac{\tan\phi'}{\tan\alpha} + \frac{c' - S_e u_w\tan\phi'}{W\cos\alpha\sin\alpha} \tag{17}$$

where $FS = 1$ corresponds to a limiting condition for equilibrium, and failure occurs when FS is less than 1.

3. Probabilistic analysis

3.1. Random field theory

Random fields are characterized by a distribution (e.g. log-normal type) and a spatial correlation structure. The present study considers the saturated hydraulic conductivity, K_s, to be log-normally distributed which is consistent with field measurements (Hoeksema and Kitanidis, 1985; Sudicky, 1986). A log-normal distribution can be easily arrived at by a non-linear transformation of the normal (Gaussian) distribution and it ensures that the random variable is always positive (Griffiths et al., 2011). Such a distribution has also been used by several investigators for modelling saturated hydraulic conductivity statistically (Fenton and Griffiths, 1993; Griffiths and Fenton, 1993; Gui et al., 2000; Srivastava et al., 2010; Santoso et al., 2011; Cho, 2012). A log-normally distributed K_s is defined by two parameters, a mean (μ_{K_s}) and coefficient of variation (ν_{K_s}) which are related by:

$$\nu_{K_s} = \frac{\sigma_{K_s}}{\mu_{K_s}} \tag{18}$$

where σ_{K_s} is the standard deviation for the log-normally distributed K_s. The equivalent parameters of the normally distributed $\ln K_s - \mu_{\ln K_s}$ and $\sigma_{\ln K_s}$ (i.e. the mean and standard deviation of $\ln K_s$) are:

$$\sigma^2_{\ln K_s} = \ln\left(1 + \nu^2_{K_s}\right) \tag{19}$$

$$\mu_{\ln K_s} = \ln\left(\mu_{K_s}\right) - \frac{1}{2}\sigma^2_{\ln K_s}. \tag{20}$$

In addition to the mean and the coefficient of variation, a third parameter, the spatial correlation length $\theta_{\ln K_s}$, is required to completely define a random field. The spatial correlation length defines the distance over which the soil properties are significantly correlated; with properties separated by a distance greater than $\theta_{\ln K_s}$ being generally uncorrelated. A large spatial correlation length means that the soil properties are highly correlated over a large distance, implying less spatial variability and more uniformity in soil properties. Conversely, a small correlation length implies a higher spatial variability and less uniformity in the soil properties. In the context of random fields, the spatial correlation lengths are generally incorporated through a correlation function. The correlation function ρ assumed for the present study is an exponential one of the form:

$$\rho(z) = \exp\left(-\frac{|z|}{\theta_{\ln K_s}}\right). \tag{21}$$

Based on the log-normal distribution and the correlation function defined above, one-dimensional random fields for saturated hydraulic conductivity K_s can be generated. In the present study, the Karhunen Loève (KL) expansion method (Zhang and Lu, 2004) is used for this purpose. Note that the required number of terms in the KL expansion

increases when the spatial correlation length decreases and, for the smallest $\theta_{\ln K_s}$ considered in this study, more than 5000 terms were used. The Karhunen Loève expansion method generates a Gaussian (normal) random field and K_s, being log-normal, requires a log-normal random field. This is obtained through the transformation:

$$K_{sj} = \exp\left(\mu_{\ln K_s} + \sigma_{\ln K_s} g_j\right) \tag{22}$$

where K_{sj} is the saturated hydraulic conductivity assigned to the jth node (of the 1D finite element mesh) and g_j is the Gaussian equivalent of K_{sj} obtained from a zero mean and unit standard deviation. The dimensionless form of spatial correlation length Θ is defined as:

$$\Theta = \frac{\theta_{\ln K_s}}{D} \tag{23}$$

where D is the length of the random field.

The exponential correlation function produces many small scale variations. In order to capture these small-scale variations, the element size needs to be sufficiently small. In the present study the smallest correlation length was 0.125 m and the element size was 0.01 m. This means that element size is 8 times smaller than the smallest spatial correlation length. It was observed that stable results can be obtained by this mesh density.

3.2. Risk assessment

During rainfall, water infiltrates into the soil from the top and can cause shallow or deep failures. It is clear that a deep failure will tend to cause more damage and thus has a more severe consequence. Therefore, the consequence associated with shallow and deep failures should be assessed individually. In the present study, consequence is assumed to be directly related to the failure depth D_f. The risk R is defined as:

$$R = \sum_{i=1}^{n_f} p_{fi} \times C_i \tag{24}$$

where p_{fi} and C_i are the probability and consequence of failure mode i, and n_f is the number of failures.[2] In applications, an additional vulnerability component would be added to Eq. (24). However, it has been assumed to be one here for simplicity and to concentrate the paper on the novel developments (e.g. Cassidy et al., 2008). Eq. (24) can be rewritten in the traditional form as:

$$R = \sum_{i=1}^{n_f} p_{fi} \times C_i = \sum_{i=1}^{n_f} \frac{1}{n_{sim}} \times C_i = \frac{1}{n_{sim}} \sum_{i=1}^{n_f} C_i = \frac{n_f}{n_{sim}} \frac{\sum_{i=1}^{n_f} C_i}{n_f} = p_f C \tag{25}$$

where C is the consequence and n_{sim} is the number of Monte-Carlo simulations.

$$p_f = \frac{n_f}{n_{sim}} \tag{26}$$

and

$$C = \frac{\sum_{i=1}^{n_f} C_i}{n_f}. \tag{27}$$

[2] For the Monte-Carlo simulations conducted in this study the rainfall duration was fixed. The factor of safety (FS) was calculated for each time step and at all depths. Whenever $FS < 1$, failure occurs and simulation stops. The time and depth of failure are then recorded. If FS is greater than 1 when rainfall stops, slope is said to be safe. The number of failures (n_f) is the sum of failures. Each failure is treated as an independent failure mode, so the probability of one single failure mode is constant, i.e. $p_{fi} = 1 / n_{sim}$. As the simulation stops whenever $FS < 1$, it is impossible for another failure to occur after one failure has happened. This means that failures are disjoint.

It can be seen from Eq. (27) that consequence C in the traditional risk definition should be redefined as the average consequence of all failures.

4. Examples

The risks associated with the failure of two slopes are assessed in this section. "Example 1" considers a purely frictional soil slope while "Example 2" considers a cohesive-frictional soil slope. It is shown that shallow failures are more likely to occur in the first example.

A hypothetical slope, at an inclination of $\alpha = 36°$ to the horizontal, is considered as shown in Fig. 1. A 1 m thick homogeneous soil layer is underlain by rock (i.e. $D = 1$ m). The water table is initially 2 m (all distances measured normal to the slope) below the ground surface and is assumed to be constant throughout the analysis. The initial pore water pressure profile is hydrostatic and, as rainfall occurs, the water is assumed to infiltrate in a wetting front normal to the slope. The rainfall intensity is I, and the flux q infiltrating the soil at the top is given by $I \cos\alpha$. No ponding of water is allowed at the ground surface at any time. The mechanical and hydraulic properties of the soil are given in Table 1 (White and Singham, 2012). In this section, the landslide risk of the slope described above is assessed for the two examples.

4.1. Example 1

In this example it is assumed that $c' = 0$. Based on the expression for the factor of safety (Eq. (17)) with the parameters described in Table 1 and considering $\alpha = 36°$, the factor of the safety before rainfall (considering a hydrostatic distribution) is 1.285.

4.1.1. Estimation of pore water pressure distribution at failure

Assuming that soil is fully saturated (i.e. $S_e = 1$) at failure, the pore water pressure required to cause failure at different depths can be estimated analytically. Substituting $FS = 1$ and $S_e = 1$ into Eq. (17) gives:

$$u_w = \frac{c' - \left(1 - \frac{\tan\phi'}{\tan\alpha}\right) W \cos\alpha \sin\alpha}{\tan\phi'}. \tag{28}$$

The initial and failure profiles of the pore water pressure are shown in Fig. 2. In this figure, "Initial condition" represents the initial hydrostatic pore water pressure distribution and "$FS = 1.00$" represents the pore water pressure (corresponding to different depths of failure) estimated from Eq. (28). The pore water pressure at failure is shown on a magnified scale in the inset. It can be observed that failures occur due to loss of suction only. The residual negative pore water pressure (at failure) increases with an increase in depth. This implies that the failure depth will depend on the reduction in the negative pore water pressure and will be the deepest when the reduction in the negative pore water pressure is the least. This is because with an increase in depth, the destabilizing force due to the weight component increases and, therefore in case of a deep failure, the negative pore water pressure need not be reduced to the same extent as that required for a shallow failure.

4.1.2. Preliminary deterministic analysis

A series of deterministic analyses is performed where I is kept constant ($I = 0.25\mu_{K_s}$) and K_s is varied. Fig. 3 shows the relationship between D_f and K_s. The first passing time of failure is shown in Fig. 4. If the mean value of saturated hydraulic conductivity μ_{K_s} is considered, the depth of failure $D_f = 1.00$ m and the first passing time of failure $t_f = 0.0855$ days. If the rainfall duration is restricted to 0.0855 days, then failures would occur only for some values of K_s which are denoted by the (red) solid lines in Figs. 3 and 4. Initially, when the failure depth is the same (i.e. $D_f = 0.01$ m), an increase in K_s will allow the flux to

Table 1
Material properties of the soil (White and Singham, 2012) considered in the present study.

Parameter	Symbol	Value	Units
Porosity	n	0.4	
Unit weight of soil solids	γ_s	20	kN/m^3
Unit weight of water	γ_w	10	kN/m^3
Mean saturated hydraulic conductivity	μ_{K_s}	8.64	m/day
Residual water content	θ_r	0.128	
Saturated water content	θ_s	0.4	
Scaling suction	a	5	1/m
Van Genuchten model parameter	N	1.5	
Van Genuchten model parameter	m	$(N-1)/N$	
Effective cohesion (Example 1/Example 2)	c'	0/0.15	kPa
Effective friction angle	ϕ'	35	°

infiltrate quickly and this explains why with an increase in K_s, the failure time decreases. However, around $K_s = 2.35$ m/day, the failure depth starts increasing with an increase in K_s. Therefore the failure time also increases until $K_s \approx 6$ m/day after which the failure time decreases again. This is because, when $K_s \approx 6$ m/day, the failure occurs at the impermeable boundary. Increasing K_s any further will not affect the failure depth (i.e. the failure will still occur at the boundary) but, will reduce the time required for the flux to infiltrate to the bottom and cause failure.

i. From Figs. 3 and 4, it can be seen that there exists a range of saturated hydraulic conductivity values between which the failure is always shallow. K_{snf} represents the lower bound and K_{smin} represents the upper bound of this range. The depth of shallow failure is minimum for K_{snf} and maximum for K_{smin}. In this range of K_s,D_f increases when K_s increases. If K_s is less than K_{snf}, there is no failure.
ii. If K_s is in between K_{smin} and μ_{K_s}, there will be no failures. In other words, no failure is observed in the soil profile between 0.77 m and 1.00 m and this shall be referred to as the "region of no failure" later on.
iii. If K_s is greater than μ_{K_s}, the failure will always be deep ($D_f = 1.00$ m).

Fig. 5 illustrates situations of deep and shallow failures, respectively, as observed in the deterministic study.

4.1.3. Analytical estimation of probability of failure

Based on the observations presented in the previous subsection, the probability of failure can be estimated analytically. Fig. 6 shows the saturated hydraulic conductivity, K_s, distributed log-normally with mean $\mu_{K_s} = 8.64$ m/day and $\nu_{K_s} = 1$. The critical values of K_{snf}, K_{smin} and μ_{K_s} are also illustrated when the rainfall duration, $t = 0.0855$ days and the rainfall intensity $I = 0.25\mu_{K_s}$.[3] For the time t, and rainfall intensity I, the probability of the saturated hydraulic conductivity K_s being below a certain value K, can then be determined analytically, by transforming the log-normal to normal as:

$$\begin{aligned} P(K_s < K) &= P(\ln K_s < \ln K) = P\left(Z < \frac{\ln K - \mu_{\ln K_s}}{\sigma_{\ln K_s}}\right) \\ &= \Phi\left(\frac{\ln K - \mu_{\ln K_s}}{\sigma_{\ln K_s}}\right) \end{aligned} \tag{29}$$

where Φ is the cumulative standard normal distribution and Z is the standard normal variate. The log-normal parameters $\mu_{\ln K_s}$ and $\sigma_{\ln K_s}$ are obtained from the parameters μ_{K_s} and σ_{K_s} as explained in Section 3.1.

The probability of failure p_f can be determined analytically as a sum of the probabilities of shallow failure p_{fs} ($D_f < 1.00$ m) and deep failure p_{fd} ($D_f = 1.00$ m). This can be written as:

$$p_f = p_{fs} + p_{fd} \tag{30}$$

where

$$\begin{aligned} p_{fs} &= P\left(K_{snf} < K_s < K_{smin}\right) \\ &= P(K_s < K_{smin}) - P\left(K_s < K_{snf}\right) \\ &= P\left(Z < \frac{\ln K_{smin} - \mu_{\ln K_s}}{\sigma_{\ln K_s}}\right) - P\left(Z < \frac{\ln K_{snf} - \mu_{\ln K_s}}{\sigma_{\ln K_s}}\right) \\ &= \Phi\left(\frac{\ln K_{smin} - \mu_{\ln K_s}}{\sigma_{\ln K_s}}\right) - \Phi\left(\frac{\ln K_{snf} - \mu_{\ln K_s}}{\sigma_{\ln K_s}}\right) \end{aligned} \tag{31}$$

$$\begin{aligned} p_{fd} &= P\left(K_s > \mu_{K_s}\right) \\ &= 1 - P\left(K_s < \mu_{K_s}\right) \\ &= 1 - P\left(Z < \frac{\ln \mu_{K_s} - \mu_{\ln K_s}}{\sigma_{\ln K_s}}\right) \\ &= 1 - \Phi\left(\frac{\ln \mu_{K_s} - \mu_{\ln K_s}}{\sigma_{\ln K_s}}\right). \end{aligned} \tag{32}$$

Substituting $K_{snf} = 0.1705$ m/day, $K_{smin} = 5.863$ m/day and $\mu_{K_s} = 8.64$ m/day in the above formulae (Eqs. (30), (31) and (32)), the probability of failure p_f can be determined analytically for a range of ν_{K_s}.

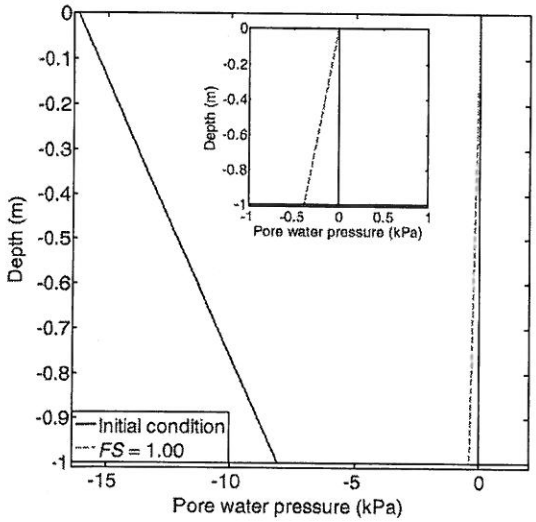

Fig. 2. Profiles of pore water pressure – initially and at failure (Example 1); inset, profile of pore water pressure at failure on a magnified scale.

[3] It is should be noted that the zoning in Fig. 6 ('No failure', 'Only shallow failure', 'Only deep failure') has been done from the results of preliminary deterministic analysis (Figs. 3 and 4), where the rainfall duration and intensity were fixed. For a given soil slope, the width of the zones will vary if the rainfall duration/intensity is changed.

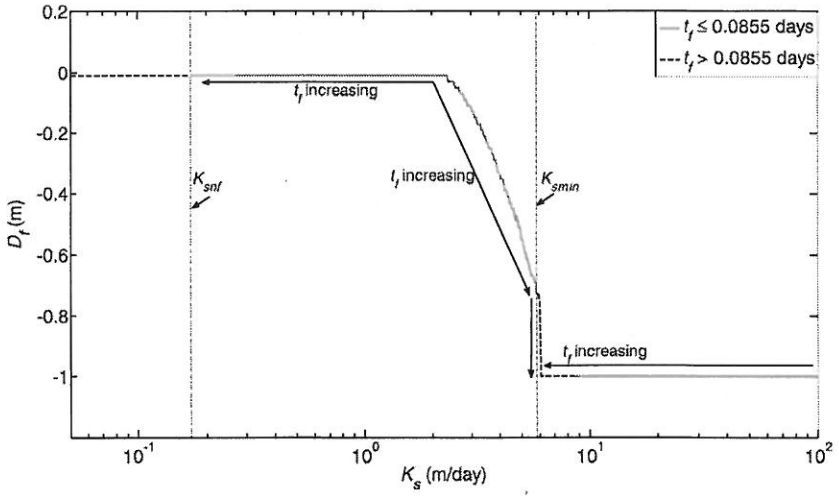

Fig. 3. Variation of failure depths D_f with saturated hydraulic conductivity K_s for $l = 0.25\mu_{K_s}$ (Example 1).

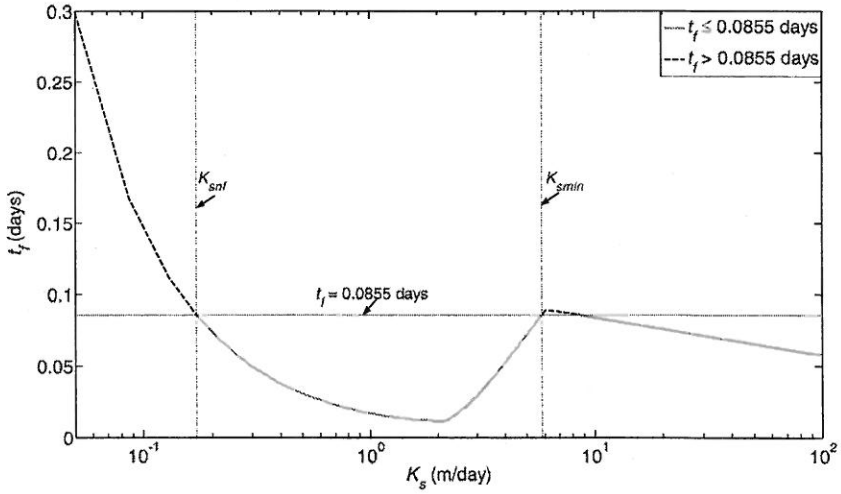

Fig. 4. Variation of first passing time of failure t_f with saturated hydraulic conductivity K_s for $l = 0.25\mu_{K_s}$ (Example 1).

4.1.4. Single-random-variable approach

To validate the analytical prediction presented in the previous subsection, a single-random-variable (SRV) analysis is conducted. The single-random-variable approach implies a very large spatial correlation length $\theta_{\ln K_s} (\approx \infty)$ i.e. the saturated hydraulic conductivity is a constant in the soil profile. The saturated hydraulic conductivity K_s is drawn at random from a log-normal distribution and assigned to the slope. For the SRV analysis, two thousand Monte Carlo simulations were performed. For each realization of K_s, seepage analysis is performed for a rainfall duration $t = 0.0855$ days. The factor of safety (FS) for every time step and depth was recorded. Whenever $FS < 1$, failure occurs and the corresponding time and depth of failure are recorded as t_f and D_f respectively. If FS is greater than 1 when rainfall stops, the slope is said to be safe, and the failure depth is recorded as zero (i.e. $D^f = 0$) in such cases. The probability of deep failure p_{fd} in this case is defined as:

$$p_{fd} = \frac{n_{fd}}{n_{sim}} \tag{33}$$

where n_{fd} is the number of failures with $D_f = 1.00$ m.[4] The probability of shallow failure p_{fs} is defined as:

$$p_{fs} = \frac{n_{fs}}{n_{sim}} = p_f - p_{fd} \tag{34}$$

where n_{fs} is the number of failures with $D_f < 1.00$ m.

The probabilities of failures p_f, p_{fs} and p_{fd} with various ν_{K_s} (0.5, 1, 1.5, 2 and 4) are compared with analytical predictions in Fig. 7. A very good agreement can be observed between the SRV results and the analytical predictions. The probability of shallow failure increases with an increase in ν_{K_s}. This is reasonable, as with an increase in ν_{K_s}, there is a shift in the log-normal distribution towards zero, thus increasing the probability of K_s being in between K_{snf} and K_{smin}. Consequently, there is a decrease in the probability of deep failures with an increase in ν_{K_s}. Thus with an increase in ν_{K_s}, the contribution of p_{fs} to p_f increases while the contribution of p_{fd} to p_f decreases. This clearly shows that the consequence should be

[4] The maximum failure depth in the present study was only 1.0 m which is referred to as a deep failure. This notion of a "deep failure" having failure depth as 1.0 m should be used in a restricted sense for the present study only. In a practical sense, such a failure would be regarded as a shallow failure.

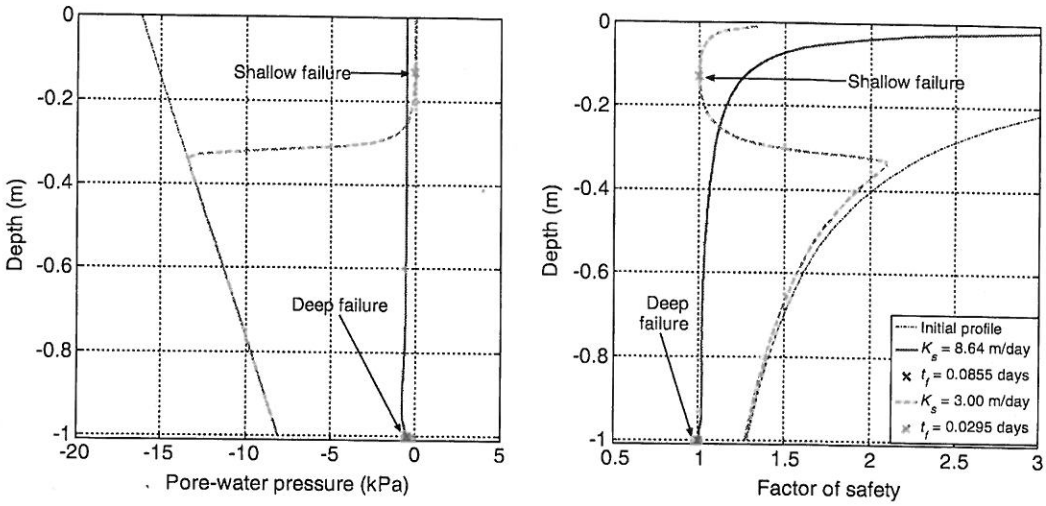

Fig. 5. Illustration of deep and shallow failures for $l = 0.25\mu_{K_s}$ and different K_s (Example 1).

assessed according to the failure mode. Otherwise, the overall risk will be incorrectly estimated.

4.1.5. Random field study

In order to investigate the effect of the spatial variability of the saturated hydraulic conductivity K_s on landslides risk, K_s is modelled as a random field while other parameters are deterministic. The probabilities of failure (p_f, p_{fs}, and p_{fd}), consequence (C), and risk (R) associated with rainfall-induced failure of the purely frictional soil slope (i.e. Example 1) are investigated. From the literature it is observed that the saturated hydraulic conductivity varies in the range of $\nu_{K_s} = 0.6$ to0.9 (Duncan, 2000). Taking the higher end of the range for the random field study, $\nu_{K_s} = 1$ is considered. Table 2 summarizes the parameters for the random field study. Two thousand Monte Carlo simulations were conducted for each spatial correlation length. For each realization of the random field of K_s, seepage analysis is performed for the duration of $t = 0.0855$ days and the results are then used to perform slope stability analysis.

The variation in failure probabilities (p_{fs}, p_{fd}, p_f), consequence (C) and risk (R) with the spatial correlation length (Θ) is shown in Fig. 8. The smallest correlation length ($\Theta = 0.125$) has the greatest spatial variability (in this study) and therefore results in the largest probability of shallow failure (p_{fs}) or the smallest probability of deep failure (p_{fd}). Since the proportion of shallow failures among the total number of failures is a maximum when $\Theta = 0.125$, the corresponding consequence is a minimum. With an increase in spatial correlation length (the soil becomes more uniform,) p_{fs} decreases while p_{fd} increases; subsequently C also increases as now more deep failures occur. Although the probability of failure p_f decreases with an increase in spatial correlation length, the risk reaches its maximum when Θ is equal to the depth of the slope i.e. $\Theta = 1.0$. This highlights the importance of individual assessment of the failure consequence.

Fig. 9 shows scatter plots of pore water pressure (u_w) at failure, for selected spatial correlation lengths Θ. The (red) solid points represent failures due to the generation of positive pore water pressures while the (blue) hollow points represent failures due to loss of suction. The solid line represents the pore water pressure at failure estimated analytically (from Eq. (28)). Firstly, the greatest scattering can be observed in the distribution of pore water pressure at failure when the spatial correlation length Θ is the smallest. Secondly, at smaller correlation lengths, slope failure may also occur due to the generation of positive pore water pressures as shown by the (red) solid points which could be attributed to non-uniformity in the weight of the failing soil mass W. As explained in Section 2.1, the weight W is obtained by integrating the unit weight γ throughout the depth to account for variations in the water content. At a smaller Θ, there is more non-uniformity

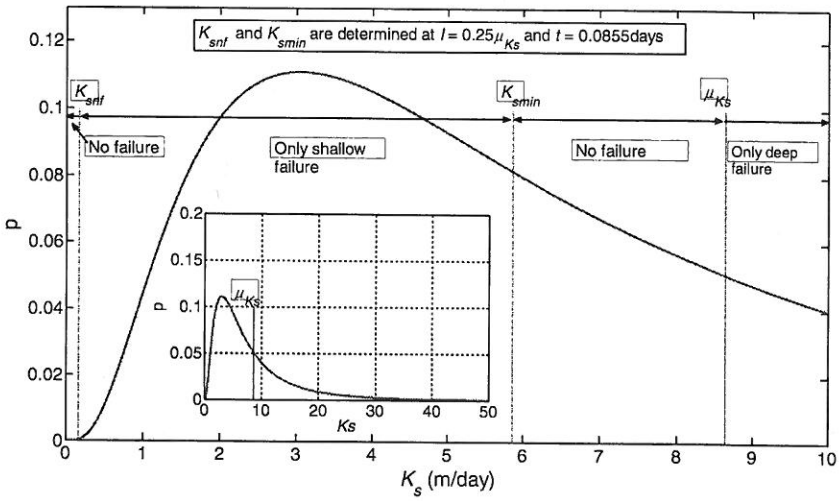

Fig. 6. Saturated hydraulic conductivity distributed log-normally with mean $\mu_{K_s} = 8.64$ m/day and $\nu_{K_s} = 1$ (Example 1) at $t = 0.0855$ days.

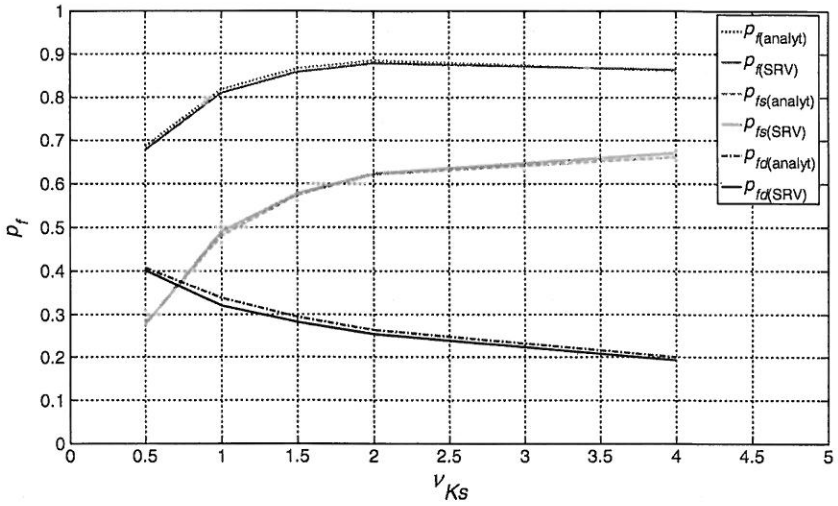

Fig. 7. Comparison of analytical estimation of failure probabilities with the SRV approach (Example 1).

(or randomness) in the weight W throughout the depth, thus requiring a greater reduction in the pore water pressure (compared to the analytical estimate) to cause failure. Thirdly, as Θ increases, the maximum depth of shallow failure also decreases. This is simply due to the soil becoming more uniform, resulting in the "region of no failure" (as explained in Section 4.1.2) becoming more prominent. Lastly, it should be noted that shallow failures can occur due to loss of suction as well and need not be due to generation of positive pore water pressures only (Santoso et al., 2011).

A noteworthy point is that the results of pore water pressure at failure start diverging from the analytical predictions as the failure depth increases. This is because the effective degree of saturation, S_e, varies with depth and is not constant as assumed in the analytical prediction of pore water pressure at failure. This can be observed in Fig. 10 which shows the scatter plots of S_e for selected spatial correlation lengths. The red (solid) points representing the locations, where $S_e = 1$, indicate that the soil was saturated at failure which implies that positive pore water pressure was generated at shallow depths. The blue (hollow) points representing the locations, where $S_e < 1$, indicate that the soil was not completely saturated or the failure occurred due to loss of matric suction.

Fig. 11 shows the histogram of failure depths for different spatial correlation lengths. More shallow failures occur for smaller correlation lengths Θ and most of these shallow failures are concentrated near the ground surface with almost zero consequence.

4.2. Example 2

In this example it is assumed that $c' = 0.15$ kPa. Based on the expression for the factor of safety (Eq. (17)) with the parameters described in Table 1 and considering $\alpha = 36°$, the factor of the safety before rainfall (considering a hydrostatic distribution) is 1.303.

Table 2
Parameters for the probabilistic study.

Parameter	Symbol	Value	Units
Mean saturated hydraulic conductivity	μ_{K_s}	8.64	m/day
Coefficient of variation	ν_{K_s}	1	
Spatial correlation length	Θ	0.125, 0.25, 0.50, 1.00, 2.00, 8.00, 100	
Length of random field	D	1	m
Number of simulations	n_{sim}	2000	

4.2.1. Estimation of pore water pressure distribution at failure

Based on Eq. (28), the pore water pressure required to cause failure at different depths can be estimated analytically. The initial and failure profiles of the pore water pressure are shown in Fig. 12. Compared to Example 1, the pore-water pressure in the top half of the soil profile is positive while the bottom half is negative at failure. This implies that failures in the top half will be due to generation of a positive pore water pressure only, whereas in the bottom half the failures can occur due to loss of suction as well.

4.2.2. Preliminary deterministic analysis

Like Example 1, a deterministic analysis is performed for Example 2 with a constant I ($= 0.25\mu_{K_s}$), and a varying K_s. To observe the variation in failure pattern, D_f and t_f are recorded for each simulation of K_s.

Fig. 13 shows the relationship between D_f and K_s. The first passing time of failure is shown in Fig. 14. If the mean value of saturated hydraulic conductivity μ_{K_s} is considered, the first passing depth of failure $D_f = 1.00$ m and the first passing time of failure $t_f = 0.0860$ days. If the rainfall duration is restricted to 0.0860 days, then failures would occur only for some values of K_s which are denoted by the (red) solid lines in Figs. 13 and 14. The only difference compared to Example 1 is in the values of K_{snf} and K_{smin}. Compared to Example 1, K_{snf} is much greater while K_{smin} is smaller in Example 2. This means that the range of K_s over which shallow failure can occur is reduced. Fig. 15 illustrates examples of deep and shallow failures as observed in the deterministic study. For Example 2, $K_{snf} = 1.253$ m/day, $K_{smin} = 3.7584$ m/day and $\mu_{K_s} = 8.64$ m/day.

4.2.3. Analytical estimation of probability of failure

Based on the results obtained in the previous section and using the expressions presented in Section 4.1.3 the probabilities of failure (p_f, p_{fs}, p_{fd}) can be analytically estimated.

4.2.4. Single-random-variable approach

Similar to Example 1, the SRV analysis is performed to determine the probabilities of failure (p_f, p_{fs}, and p_{fd}) for selected values of ν_{K_s} (0.5, 1, 1.5, 2 and 4). Two thousand Monte-Carlo simulations are performed for each ν_{K_s}. For each realization of K_s, seepage analysis is performed for a rainfall duration $t = 0.0860$ days and then the results of pore water pressure are incorporated in Eq. (17) to check for failure. The probabilities of failures p_f, p_{fs} and p_{fd} with various ν_{K_s} (0.5, 1, 1.5, 2 and 4) are compared with analytical predictions in Fig. 16. A very good agreement can be observed between the SRV results and the

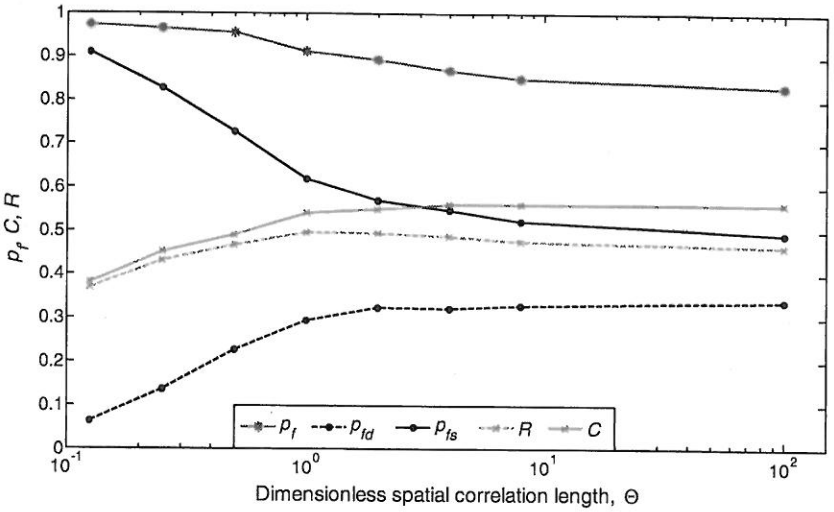

Fig. 8. Variation of failure probabilities, consequence and risk with spatial correlation lengths (Example 1).

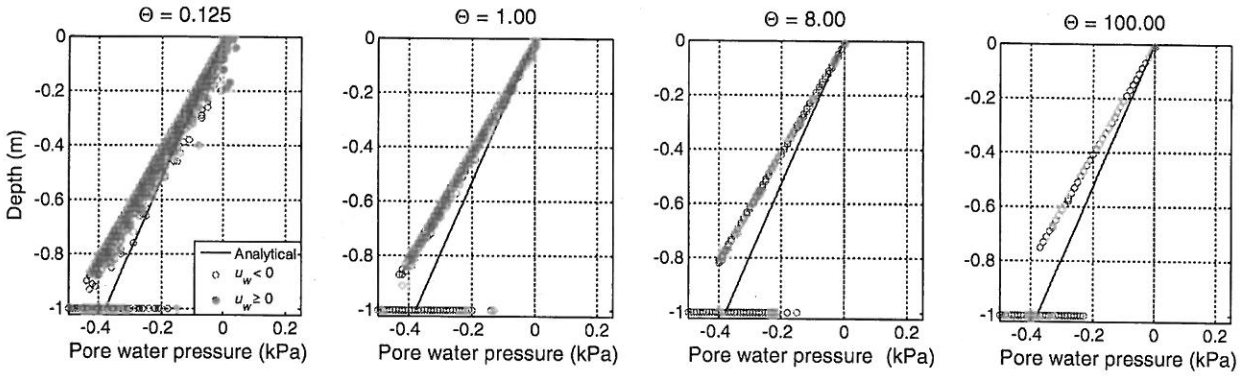

Fig. 9. Scatter plots of pore water pressure at failure for selected spatial correlation lengths (Example 1).

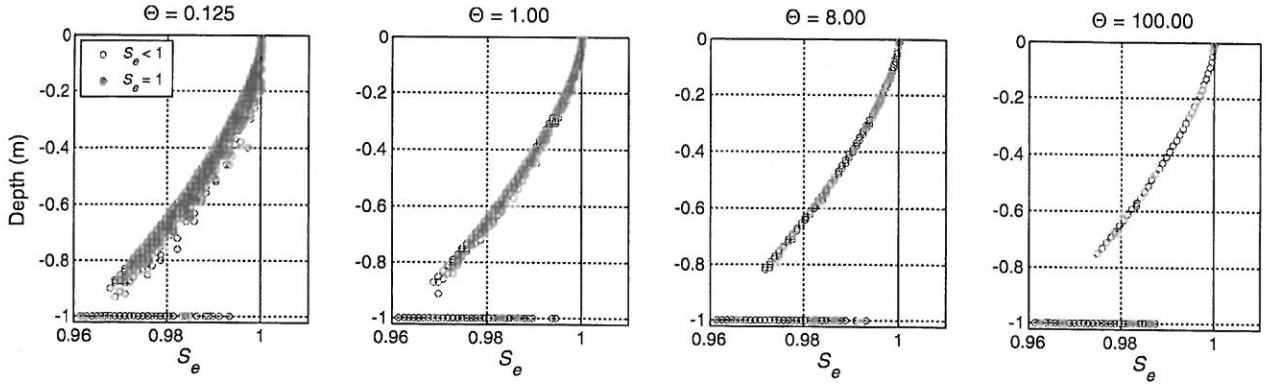

Fig. 10. Scatter plots of effective degree of saturation (S_e) at failure, for selected spatial correlation lengths (Example 1).

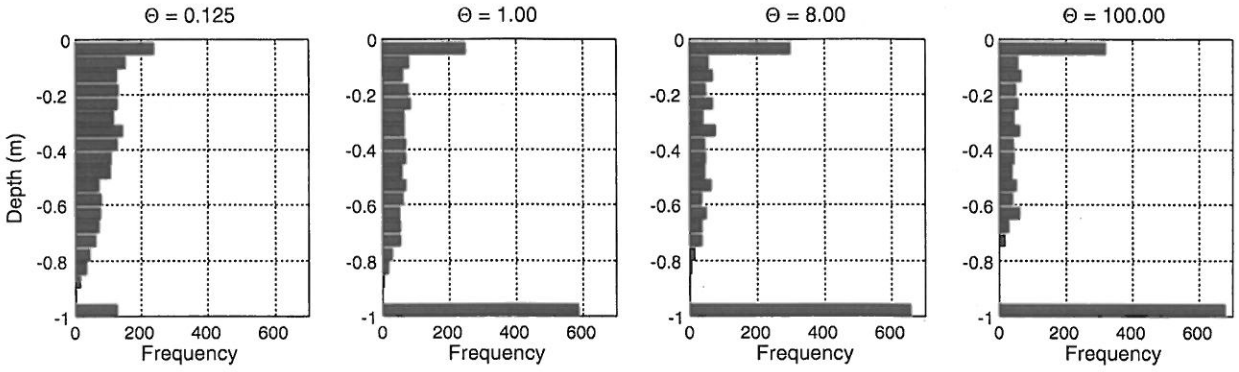

Fig. 11. Histogram of failure depths for selected spatial correlation lengths (Example 1).

analytical predictions. In Example 1, p_f increased with an increase in ν_{K_s}, reached a peak (at $\nu_{K_s} = 2$) and then decreased marginally (at $\nu_{K_s} = 4$); on the other hand, p_{fs} increased continuously while p_{fd} decreased continuously with an increase in ν_{K_s}. For Example 2, p_f increases with an increase in ν_{K_s} and reaches a peak (at $\nu_{K_s} = 1.5$) then decreases sharply; the magnitude of p_f being much smaller for each value of ν_{K_s} compared to Example 1. Unlike Example 1 where p_{fs} continuously increased with ν_{K_s}, p_{fs} for Example 2 reaches a peak (at $\nu_{K_s} = 1.5$) and then decreases. Interestingly, p_{fd} varies exactly in the same manner for both the cases within the same range of values as well. This implies that, due to a change in the triggering mechanism, there are fewer shallow failures for Example 2, resulting in a reduction in p_{fs}. Consequently, this results in a decrease in the overall probability of failure p_f as well.

4.2.5. Random field study

The parameters for the random field simulation in Example 2 are the same as in Example 1, only the soil cohesion c' is changed to 0.15 kPa for the slope stability assessment. The purpose here is to observe the effect of a change in the triggering mechanism on the failure probabilities (p_f, p_{fs}, and p_{fd}), consequence (C), and risk (R). The seepage analysis is performed for duration of $t = 0.0860$ days and the results are then used to perform slope stability analysis.

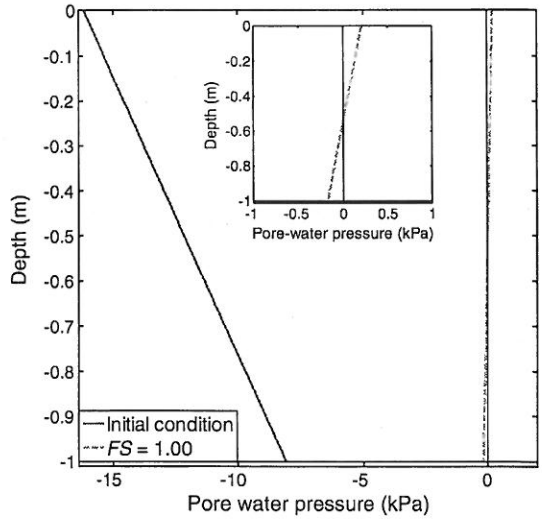

Fig. 12. Profiles of pore water pressure – initially and at failure (Example 2); inset, profile of pore water pressure at failure on a magnified scale.

Fig. 17 shows the variation in the failure probabilities (p_{fs}, p_{fd}, p_f), consequence (C) and risk (R) with spatial correlation length (Θ). Compared to Example 1, although the trend in the variation of the failure probabilities with Θ is somewhat similar, the variation occurs over a different range of values with a significant reduction in p_{fs} at all values of Θ. This reduction can be attributed to a different triggering mechanism (i.e. generation of a positive pore water pressure) which causes fewer shallow failures. The variation in p_{fd} is very similar to Example 1. Therefore, the reduction in p_f is primarily due to a reduction in p_{fs}. The consequence is a minimum for $\Theta = 0.125$ and increases with Θ as the soil becomes more uniform, similar to what was observed in Example 1. However, deeper shallow failures cause an increase in the consequence C compared to Example 1. The risk R depends on p_f and C, and p_f decreases while C increases with Θ. Subsequently, a maximum risk can be observed at $\Theta = 0.50$, implying that a critical spatial correlation length exists at which the risk is greatest. The variation in the risk R with Θ occurs over a very narrow range (in Example 2) with a higher risk being observed at smaller spatial correlation lengths ($\Theta = 0.125, 0.25, 0.5$) compared to Example 1.

Fig. 18 shows the distribution of pore water pressure (u_w) at failure plotted against the corresponding failure depths D_f for different spatial correlation lengths Θ. The (red) solid points represent failures due to the development of positive pore water pressure while the (blue) hollow points represent failures due to a loss of suction. The solid line represents the pore water pressure at failure estimated analytically (from Eq. (28)). A significant scatter can be observed in the results (of u_w) for small correlation lengths (Θ). The scatter decreases with an increase in Θ, similar to that observed for Example 1. However, in contrast to Example 1, where most of the surficial failures are due to loss of suction, the shallow failures in the top half of the soil profile are only due to generation of a positive pore water pressure. Also, few failures at the bottom occur due to generation of a positive pore water pressure, which was not observed in Example 1. The number of failures occurring due to positive pore water pressure generation is greatest for the smallest Θ, and decreases with an increase in Θ. As Θ increases, the number of shallow failures occurring near the surface also starts decreasing which causes a decrease in p_{fs} as observed in Fig. 17. The development of positive pore water pressure is also confirmed in Fig. 19, which shows scatter plots of S_e at failure for selected spatial correlation lengths. The (red) solid points representing the locations, where $S_e = 1$, indicate that the soil was saturated at failure which implies that positive pore water pressure was generated at shallow depths. The (blue) hollow points representing the locations, where $S_e < 1$, indicate that the soil was not completely saturated or the failure occurred due to loss of matric suction. Fig. 20 illustrates examples of shallow and deep failures occurring due to generation of a positive pore water pressure for the random fields shown in Fig. 21.

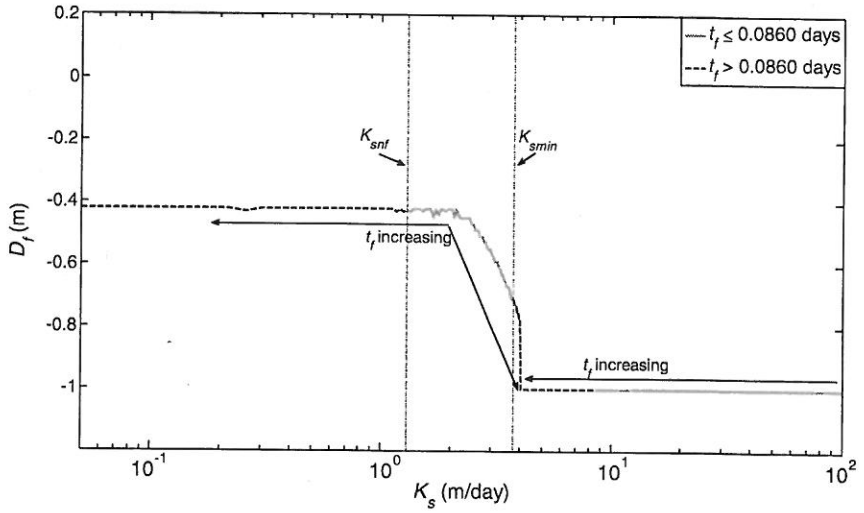

Fig. 13. Variation of failure depths D_f with saturated hydraulic conductivity K_s for $I = 0.25\mu_{K_s}$ (Example 2).

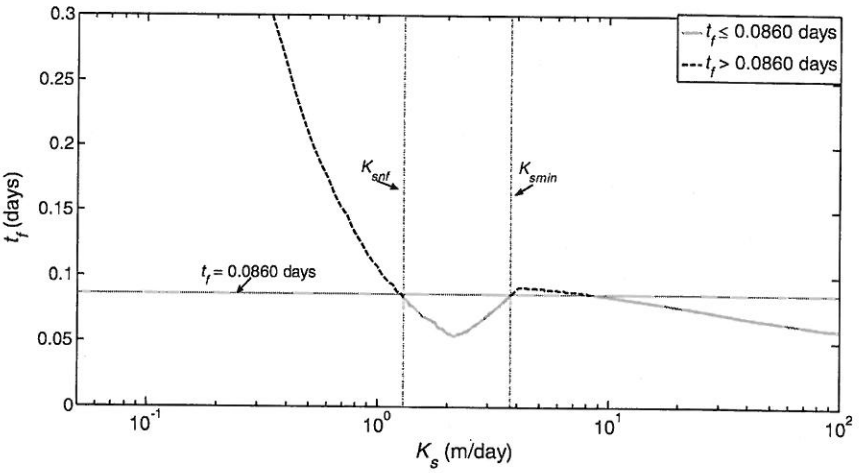

Fig. 14. Variation of first passing time of failure t_f with saturated hydraulic conductivity K_s for $I = 0.25\mu_{K_s}$ (Example 2).

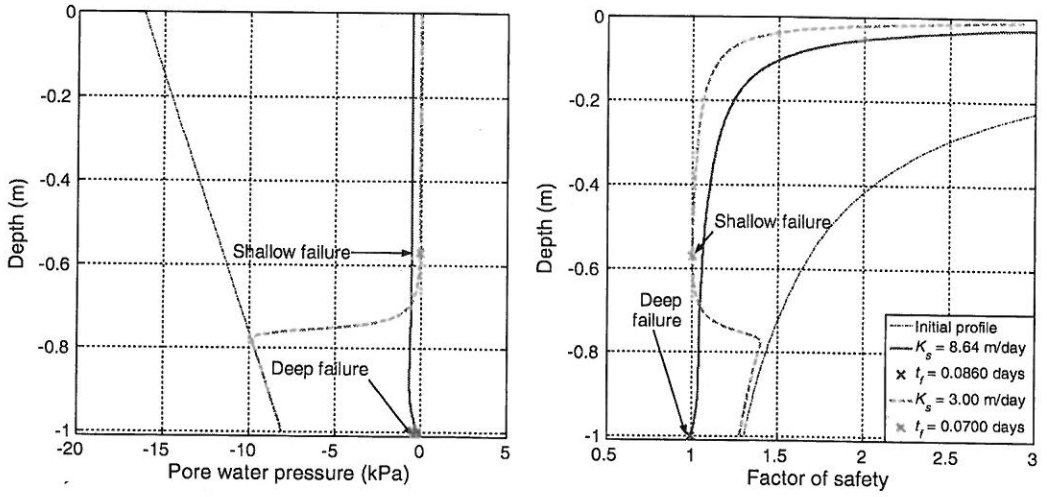

Fig. 15. Illustration of deep and shallow failures for $I = 0.25\mu_{K_s}$ and different K_s (Example 2).

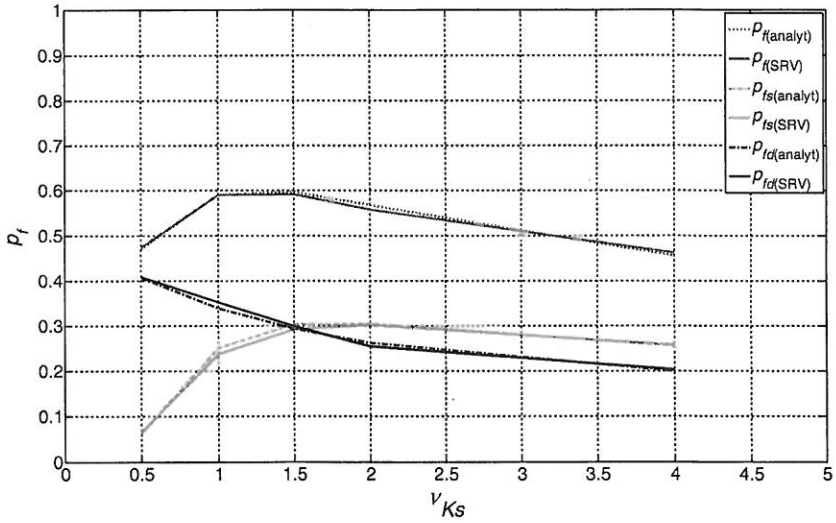

Fig. 16. Comparison of analytical estimation of failure probabilities with the SRV approach (Example 2).

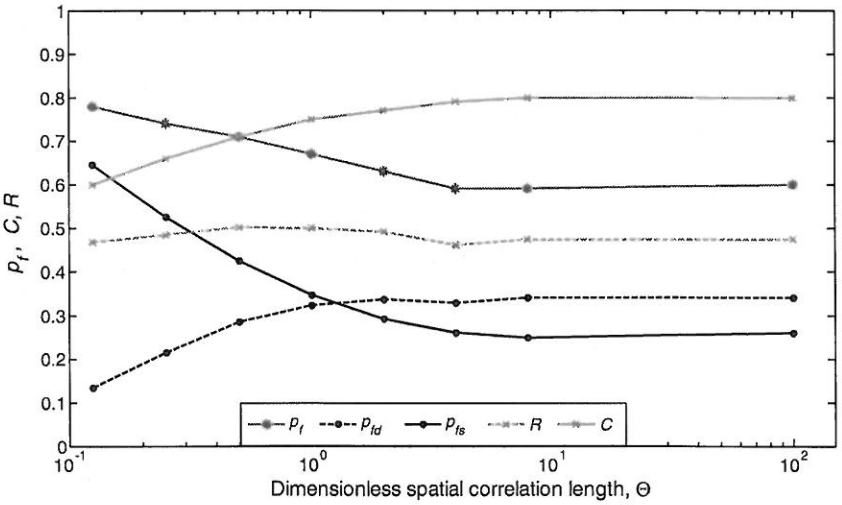

Fig. 17. Variation of failure probabilities, consequence and risk with spatial correlation lengths (Example 2).

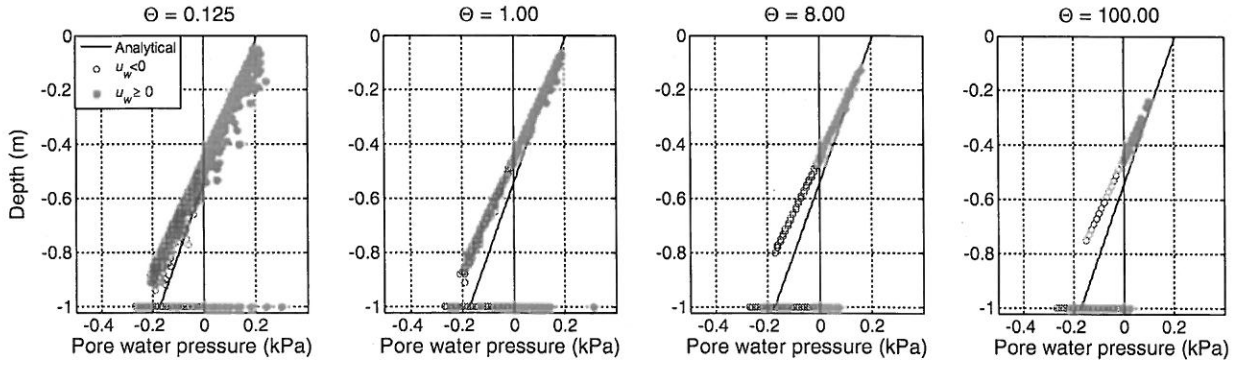

Fig. 18. Scatter plots of pore water pressure at failure for selected spatial correlation lengths (Example 2).

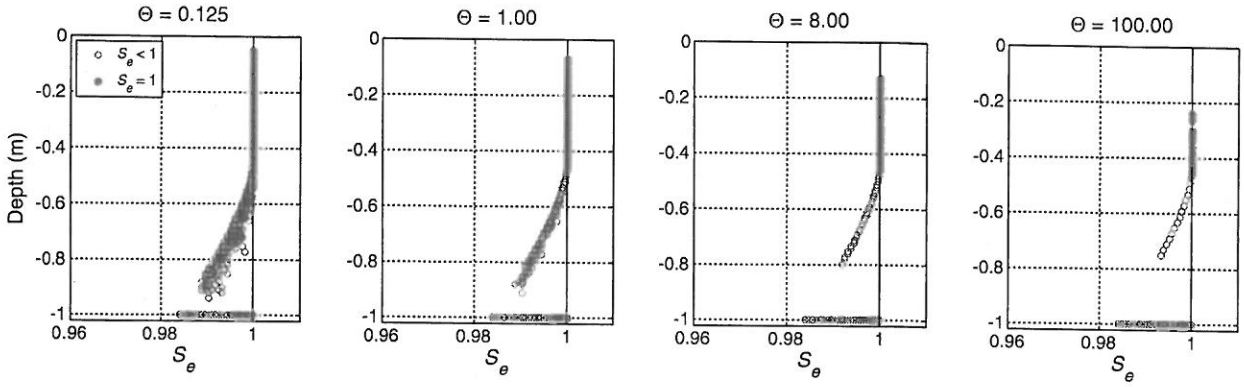

Fig. 19. Scatter plots of effective degree of saturation (S_e) at failure, for selected spatial correlation lengths (Example 2).

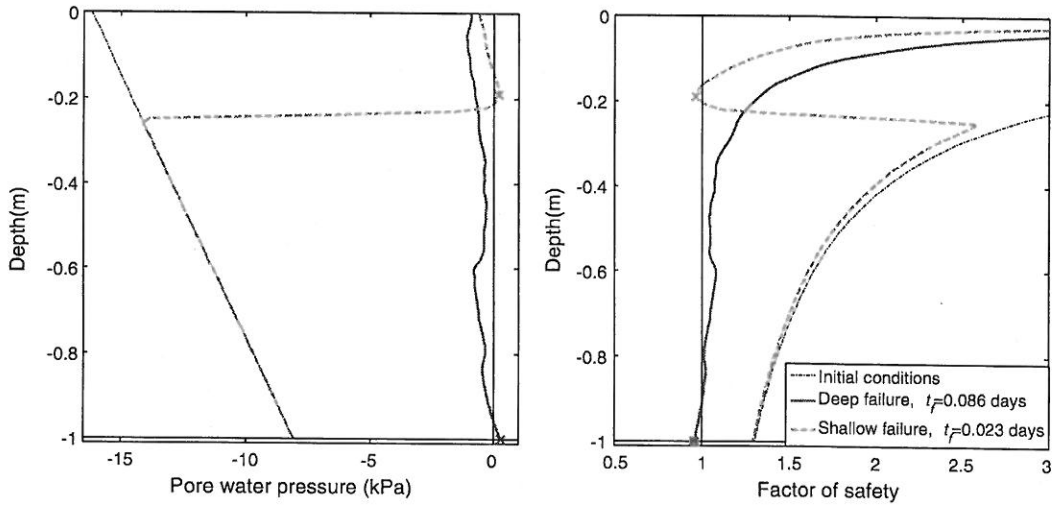

Fig. 20. Illustration of shallow and deep failures due to generation of a positive pore water pressure (Example 2).

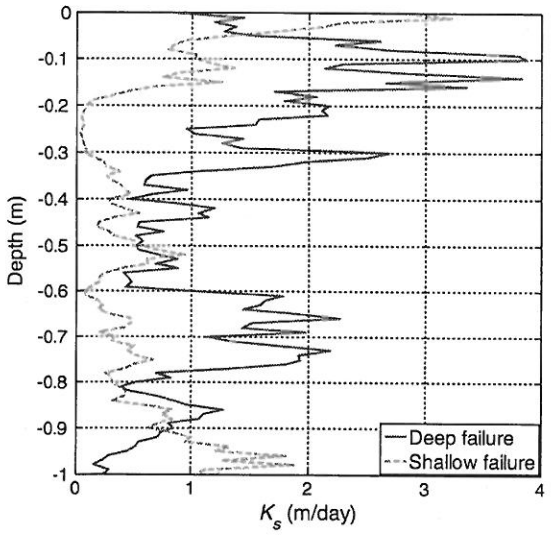

Fig. 21. Sample random fields for deep and shallow failures due to generation of positive pore water pressures (Θ = 0.125).

Fig. 22 shows the histogram of failure depths D_f for different spatial correlation lengths Θ. As far as shallow failures are concerned, they are much deeper in Example 2 compared to Example 1 at all spatial correlation lengths. The histogram clearly illustrates the reason for an increase in consequence compared to Example 1, as the shallow failures are much deeper.

5. Conclusion

The risk of rainfall induced landslides is studied quantitatively, based on the logic that the consequence should be assessed individually for each failure. When the saturated hydraulic conductivity is modelled as a random field, it was shown that the probability of failure increases as the spatial correlation length increases. However, when consequence of failure (measured here by the depth of the failure) is accounted for, a critical spatial correlation length exists at which the risk is maximum. This confirms clearly that the consequence should be assessed individually for a rational risk assessment. The triggering mechanisms for a rainfall induced landslide have also been highlighted by the pore water pressure distributions at failure. When failure occurs due to generation of positive pore water pressure, the risk tends to be higher than when the failure occurs due to loss of suction.

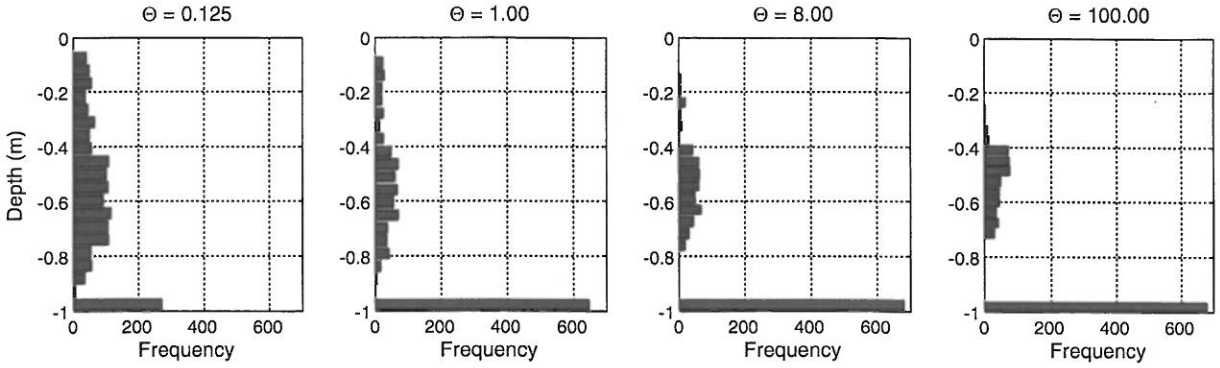

Fig. 22. Histogram of failure depths for selected spatial correlation lengths (Example 2).

6. Notations

a	scaling suction
c'	effective cohesion
C	consequence
D	slope depth
D_f	depth of failure
F_N	normal force
F_T	tangential force
FS	factor of safety
g	gaussian equivalent of the log-normal saturated hydraulic conductivity random field
I	rainfall intensity
K	hydraulic conductivity
K_r	relative hydraulic conductivity
K_s	saturated hydraulic conductivity
K_{smin}	maximum value of K_s which can cause a shallow failure
K_{snf}	minimum value of K_s which can cause a shallow failure
m	van Genuchten model parameter
n	soil porosity
n_f	number of simulations resulting in slope failures
n_{sim}	number of simulations
n_{fd}	number of simulations resulting in deep slope failures
n_{fs}	number of simulations resulting in shallow slope failures
N	van Genuchten model parameter
p_f	probability of failure
p_{fd}	probability of deep failure
p_{fs}	probability of shallow failure
q	flux infiltrating the slope
R	risk
S	degree of saturation
S_e	effective degree of saturation
S_r	residual degree of saturation
t	rainfall duration
t_f	first passing time of failure
u	pore pressure head
u_w	pore water pressure
u_a	pore air pressure
W	weight of failing soil mass
z	slope normal direction
Z	standard normal variate
α	slope angle
γ	unit weight of soil
γ_s	unit weight of soil solids
γ_w	unit weight of water
θ	soil volumetric water content
θ_r	residual water content
θ_s	saturated water content
$\theta_{\ln K_s}$	spatial correlation length of logarithm of saturated hydraulic conductivity
Θ	normalized spatial correlation length of logarithm of saturated hydraulic conductivity
μ_{K_s}	mean saturated hydraulic conductivity
$\mu_{\ln K_s}$	mean of logarithm of saturated hydraulic conductivity
ν_{K_s}	coefficient of variation of saturated hydraulic conductivity
$\rho(z)$	correlation function
σ	total normal stress
σ'	effective normal stress
σ_{K_s}	standard deviation of saturated hydraulic conductivity
$\sigma_{\ln K_s}$	standard deviation of logarithm of saturated hydraulic conductivity
τ	soil shear stress
τ_f	soil shear strength
ϕ'	effective friction angle
Φ	cumulative standard normal distribution function
χ	coefficient of effective stress

Acknowledgements

The authors wish to acknowledge the support of the Australian Research Council (CE11001009) in funding the Centre of Excellence for Geotechnical Science and Engineering.

References

Bishop, A.W., 1959. The effective stress principle. Teknisk Ukeblad 39, 859–863.
Brand, E.W., 1984. Landslides in South Asia: a state-of-art report. 4th International Symposium on Landslides, Toronto.
Cassidy, M.J., Uzielli, M., Lacasse, S., 2008. Probability risk assessment of landslides: a case study at Finneidfjord. Can. Geotech. J. 45 (9), 1250–1267.
Cho, S.E., 2012. Probabilistic analysis of seepage that considers the spatial variability of permeability for an embankment on soil foundation. Eng. Geol. 133–134, 30–39.
Cho, S.E., 2014. Probabilistic stability analysis of rainfall-induced landslides considering spatial variability of permeability. Eng. Geol. 171, 11–20.
Collins, B.D., Znidarcic, D., 2004. Stability analyses of rainfall induced landslides. J. Geotech. Geoenviron. 130 (4), 362–372.
DeGroot, D.J., Baecher, G.B., 1993. Estimating autocovariance of in-situ soil properties. J. Geotech. Eng. 119 (1), 147–166.
Duncan, J.M., 1996. State of the art: limit equilibrium and finite-element analysis of slopes. J. Geotech. Eng. 122 (7), 577–596.
Duncan, J.M., 2000. Factors of safety and reliability in geotechnical engineering. J. Geotech. Geoenviron. 126 (4), 307–316.
Fenton, G.A., Griffiths, D.V., 1993. Statistics of block conductivity through a simple bounded stochastic medium. Water Resour. Res. 29 (6), 1825–1830.
Fourie, A.B., 1996. Predicting rainfall-induced slope instability. Proceedings of the ICE-Geotechnical Engineering, 119(4), pp. 211–218.
Fredlund, D.G., Rahardjo, H., 1993. Soil Mechanics for Unsaturated Soils. John Wiley & Sons, Inc., New York.
Griffiths, D.V., Fenton, G.A., 1993. Seepage beneath water retaining structures founded on spatially random soil. Geotechnique 43 (4), 577–587.

Griffiths, D.V., Huang, J., Fenton, G.A., 2011. Probabilistic infinite slope analysis. Comput. Geotech. 38 (4), 577–584.
Gui, S., Zhang, R., Turner, J.P., Xue, X., 2000. Probabilistic slope stability analysis with stochastic soil hydraulic conductivity. J. Geotech. Geoenviron. 126 (1), 1–9.
Hoeksema, R.J., Kitanidis, P.K., 1985. Analysis of the spatial structure of properties of selected aquifers. Water Resour. Res. 21 (4), 563–572.
Huang, J., Griffiths, D.V., Fenton, G.A., 2010. Probabilistic analysis of coupled soil consolidation. J. Geotech. Geoenviron. 136 (3), 417–430.
Huang, J., Lyamin, A.V., Griffiths, D.V., Krabbenhøft, K., Sloan, S.W., 2013. Quantitative risk assessment of landslide by limit analysis and random fields. Comput. Geotech. 53, 60–67.
Lacasse, S., Nadim, F., 1996. Uncertainties in characterizing soil properties. Uncertainty in the Geologic Environment — From Theory to Practice, Madison, Wisconsin, USA, ASCE GSP No. 58.
Li, W.C., Lee, L.M., Cai, H., Li, H.J., Dai, F.C., Wang, M.L., 2013. Combined roles of saturated permeability and rainfall characteristics on surficial failure of homogeneous soil slope. Eng. Geol. 153, 105–113.
Rahardjo, H., Lim, T.T., Chang, M.F., Fredlund, D.G., 1995. Shear-strength characteristics of a residual soil. Can. Geotech. J. 32 (1), 60–77.
Rahardjo, H., Ong, T., Rezaur, R., Leong, E., 2007. Factors controlling instability of homogeneous soil slopes under rainfall. J. Geotech. Geoenviron. 133 (12), 1532–1543.
Rahimi, A., Rahardjo, H., Leong, E.C., 2010. Effect of hydraulic properties of soil on rainfall-induced slope failure. Eng. Geol. 114 (3–4), 135–143.
Richards, L.A., 1931. Capillary conduction of liquids through porous mediums. Physics 1 (5), 318–333.
Santoso, A.M., Phoon, K.K., Quek, S.T., 2011. Effects of soil spatial variability on rainfall-induced landslides. Comput. Struct. 89 (11–12), 893–900.
Simunek, J., van Genuchten, M.T., Sejna, M., 2013. The Hydrus-1D software package for simulating the movement of water, heat, and multiple solutes in variably saturated media, Version 4.16, HYDRUS Software Series 3. Department of Environmental Sciences, University of California Riverside, Riverside, California, USA, p. 340.
Srivastava, A., Babu, G.L.S., Haldar, S., 2010. Influence of spatial variability of permeability property on steady state seepage flow and slope stability analysis. Eng. Geol. 110 (3–4), 93–101.
Sudicky, E.A., 1986. A natural gradient experiment on solute transport in a sand aquifer: spatial variability of hydraulic conductivity and its role in the dispersion process. Water Resour. Res. 22 (13), 2069–2082.
Tsai, T.L., 2011. Influences of soil water characteristic curve on rainfall-induced shallow landslides. Environ. Earth Sci. 64 (2), 449–459.
Tsai, T.L., Chen, H.F., 2010. Effects of degree of saturation on shallow landslides triggered by rainfall. Environ. Earth Sci. 59 (6), 1285–1295.
Tsaparas, I., Rahardjo, H., Toll, D.G., Leong, E.C., 2002. Controlling parameters for rainfall-induced landslides. Comput. Geotech. 29 (1), 1–27.
van Genuchten, M.T., 1980. A closed-form equation for predicting the hydraulic conductivity of unsaturated soils. Soil Sci. Soc. Am. J. 44 (5), 892–898.
Vanapalli, S.K., Fredlund, D.G., Pufahl, D.E., Clifton, A.W., 1996. Model for the prediction of shear strength with respect to soil suction. Can. Geotech. J. 33 (3), 379–392.
White, J.A., Singham, D.I., 2012. Slope stability assessment using stochastic rainfall simulation. Procedia Comput. Sci. 9, 699–706.
Zhan, T.L.T., Jia, G.W., Chen, Y.M., Fredlund, D.G., Li, H., 2012. An analytical solution for rainfall infiltration into an unsaturated infinite slope and its application to slope stability analysis. Int. J. Numer. Anal. Methods Geomech. 37 (12), 1737–1760.
Zhang, D., Lu, Z., 2004. An efficient, high-order perturbation approach for flow in random porous media via Karhunen–Loève and polynomial expansions. J. Comput. Phys. 194 (2), 773–794.
Zhang, L.L., Zhang, J., Zhang, L.M., Tang, W.H., 2011. Stability analysis of rainfall-induced slope failure: a review. Proceedings of the Institution of Civil Engineers–Geotechnical Engineering, 164(5), pp. 299–316.
Zhang, S., Zhang, L.M., Peng, M., Zhang, L.L., Zhao, H.F., Chen, H.X., 2012. Assessment of risks of loose landslide deposits formed by the 2008 Wenchuan earthquake. Nat. Hazards Earth Syst. Sci. 12 (5), 1381–1392.
Zhang, J., Huang, H.W., Zhang, L.M., Zhu, H.H., Shi, B., 2014. Probabilistic prediction of rainfall-induced slope failure using a mechanics-based model. Eng. Geol. 168, 129–140.
Zhu, H., Zhang, L.M., Zhang, L.L., Zhou, C.B., 2013. Two-dimensional probabilistic infiltration analysis with a spatially varying permeability function. Comput. Geotech. 48, 249–259.